Southern African Pyrometallurgy 2011, Edited by R.T. Jones & P. den Hoed,
Southern African Institute of Mining and Metallurgy, Johannesburg, 6–9 March 2011

Thermal conductivity of solidified manganese-bearing slags—A preliminary investigation

J.D. Steenkamp, M. Tangstad, and P.C. Pistorius
University of Pretoria, Pretoria, South Africa
Norwegian University of Science and Technology, Trondheim, Norway
Carnegie-Mellon University, Pittsburgh, USA

Keywords: Thermal, conductivity, diffusivity, expansion, history, density, specific heat capacity, industrial rich high-carbon manganese slag

Abstract – The thermal conductivity of slag is an important parameter in the design of furnace-containment systems based on freeze-lining technology. Literature indicates that the crystal content of a slag has a significant influence on its thermal conductivity. Industrial, rich, manganese-bearing slag was cooled at different rates to create samples with different microstructures. The coefficients of thermal conductivity of these samples were measured in a nitrogen atmosphere from room temperature to 990°C at 100°C intervals. The laser-flash measurement technique was used for this purpose. Follow-up investigations included XRF and XRD and modelling in FACTSage.

INTRODUCTION

Freeze linings in manganese ferroalloy furnaces

Manganese ferroalloys are produced commercially in blast furnaces and submerged-arc furnaces (SAF) world-wide.[1] From the perspective of slag chemistry, three distinct processes are in operation:

- High-carbon ferromanganese (HCFeMn) production that uses a rich-slag practice
- HCFeMn production that uses a *discard*-slag practice
- Silicomanganese (SiMn) production

SAF technology is applied in all three types of process. Typical compositions of slag from the different processes are summarised in Table I.[2] The slag basicity—calculated as B_2 according to Equation 1 and B_5 according to Equation 2—is reported in Table I. B_5 is the definition of basicity generally referred to in the literature on the production of manganese ferroalloys. B_2 is the definition of basicity referred to in Figure 5 of this paper.

$$B_2 = \frac{CaO}{SiO_2} \quad [1]$$

$$B_5 = \frac{CaO + MgO + MnO}{Al_2O_3 + SiO_2} \quad [2]$$

Table I: Typical chemical compositions (per cent by mass) of slag produced in the making of manganese ferroalloys (after Olsen *et al.*[2])

	SiO_2	Al_2O_3	MnO	MgO	CaO	B_2	B_5	T_{sol}† (°C)	T_{liq}† (°C)
HCFeMn—rich	24	13	40	6	17	0.7	1.7	1118	1447
HCFeMn—discard	24	21	15	5	35	1.5	1.2	1150	1403
SiMn	45	16	9	9	21	0.5	0.6	1059	1235

† The solidus (T_{sol}) and liquidus (T_{liq}) temperature of each slag composition, as calculated with FACTSage 6.1 and the FACT53 and FToxid databases.

In SAF-process containment systems (consisting typically of a shell and lining), freeze-lining technology is widely applied when producing manganese ferroalloys.[3, 4] Figure 1 gives a schematic overview of a SAF from a furnace containment perspective. It is important to note that in manganese-ferroalloy production the slag layer is usually not as clearly defined as in Figure 1.

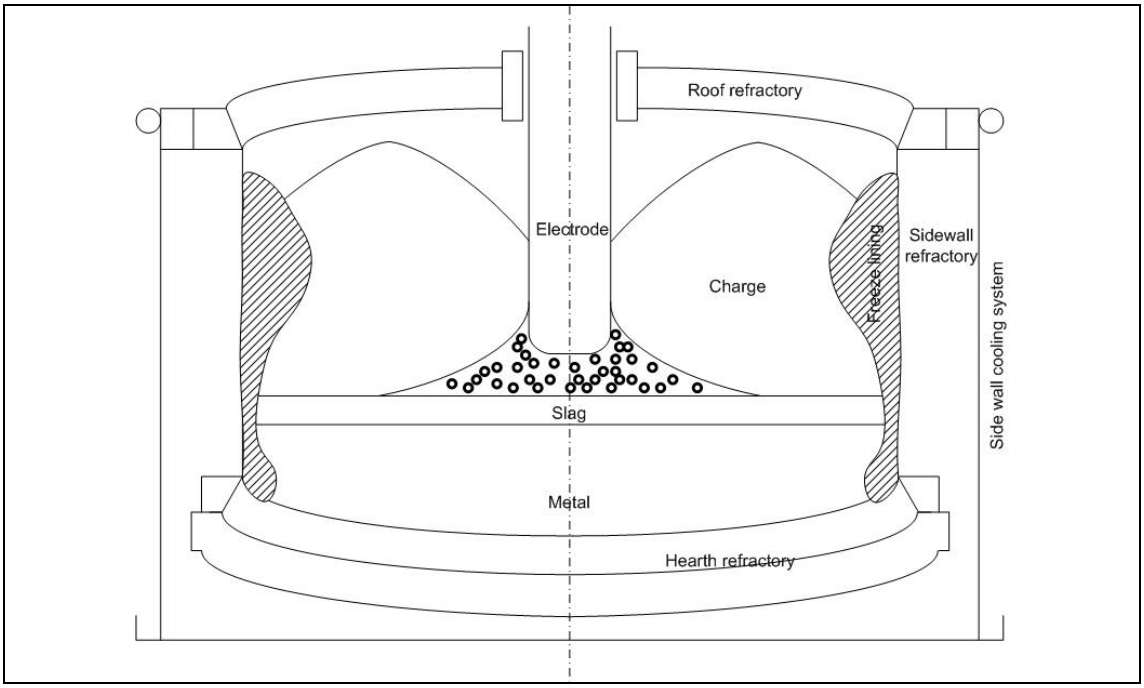

Figure 1: Conceptual layout of a SAF indicating the position of the freeze lining (after Matyas *et al.*[7]).

The sampling of freeze-linings in pilot- and industrial-scale furnaces utilised for the production of manganese ferroalloys is difficult. In pilot-scale furnaces one has the advantage of cooling the furnace down before digout, but how can one be sure that the freeze-lining one samples formed from a liquid slag—the definition of a true freeze-lining?[6] In industrial-scale furnaces the digout of a furnace commences while the furnace is still red hot owing to a requirement that the downtime for relining be kept to a minimum to save money. Obtaining a sample of the freeze-lining is therefore not possible.

To understand the morphology of a freeze-lining, laboratory-scale investigations similar to those conducted by Campforts *et al.* are required.[10] In

their investigations, a forced-cooled metal finger is submerged in a rotating bath of liquid slag (industrial or synthetic) for various lengths of time. When the cooled finger with frozen slag is removed from the bath and cooled, the slag layer is investigated further. Figure 2 depicts an example of a freeze-lining formed in this manner. The freeze-lining was formed by submerging a forced cooled finger in a six-component, synthetic lead slag for 120 minutes. Note the complex layers of glass and crystals.

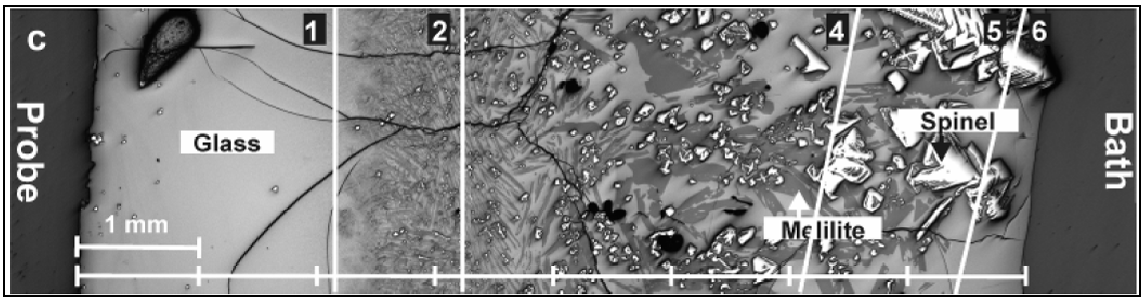

Figure 2: Image by light optical microscopy of a six-component, synthetic lead slag freeze-lining produced by Campforts *et al.* using a cooled probe technique.

Freeze-linings and the thermal conductivity of slag

Several parameters influence the thickness of the freeze-lining, one of them being the thermal conductivity of the frozen slag. In Figure 3 the effect of the thermal conductivity of solid slag on freeze-lining thickness is illustrated for thermal conductivities of 1 and 3 $W.m^{-2}.K^{-1}$. The details of the calculation are reported elsewhere.[8] This type of calculation is used when designing furnace containment systems.

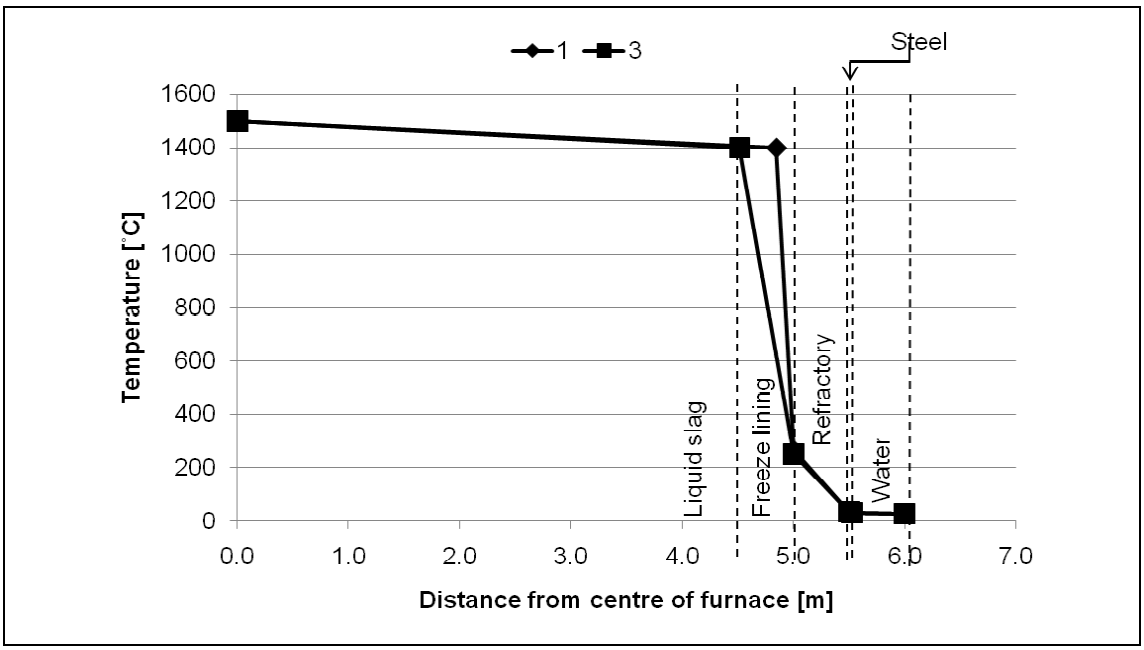

Figure 3: Thermal profile as a function of distance from steel-shell cold face. Coefficients of thermal conductivity for slag, 1 and 3 $W.m^{-2}.K^{-1}$, respectively. The coefficient of convection of the slag was taken as 75 $W.m^{-2}.K^{-1}$ based on the data published by Duncanson and Toth.[8]

Slag with a thermal conductivity of 1 $W.m^{-2}.K^{-1}$ will result in a freeze lining thickness of 153 mm, and 3 $W.m^{-2}.K^{-1}$ in 483 mm (see Figure 3). From this

illustration it may be concluded that, when designing a furnace containment system, one should quantify the coefficient of thermal conductivity of the specific slag found in the process. Furthermore the factors that can influence thermal conductivity should be understood.

According to Mills and Susa[9] the thermal conductivity of slag depends on—

1. The temperature of the slag (Figure 4 and Figure 5)
2. The crystal content of the slag (Figure 4)
3. The chemical composition of the slag (Figure 5), more specifically its basicity as defined in Equation 1

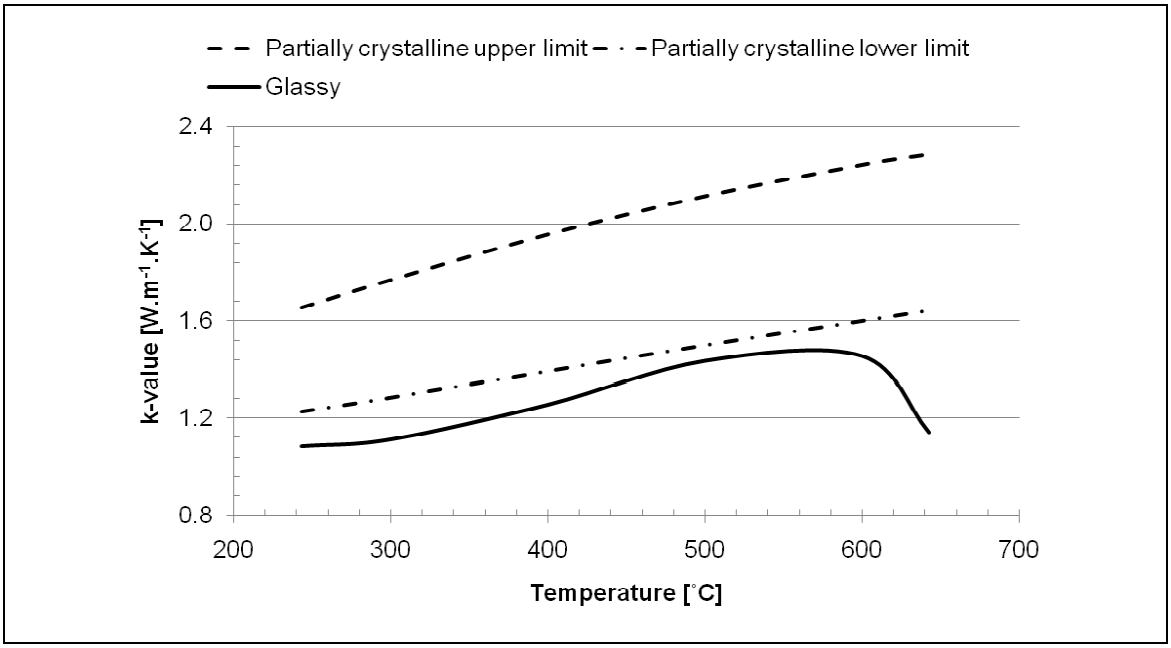

Figure 4: Measured thermal conductivities of continuous casting slags indicating the effect of crystal content and temperature on the thermal conductivity of the slag—redrawn from Mills and Susa.[9]

To illustrate that not only the crystal content of the slag influence its thermal conductivity, the liquidus and solidus temperatures of slags with varying basicity were calculated in FACTSage 6.1 with the FACT53 and FToxid databases. The temperatures have been added to Figure 5.

Factors influencing the thermal conductivity of slag

Given the fact that the thermal conductivity of slag changes with temperature (Figure 4 and Figure 5) and the fact that slag-lining thicknesses are often reported[3] as having been calculated for a constant value of thermal conductivity—as for the results in Figure 3—we pose the question, to what extent would the *temperature* of *manganese-bearing* slag influence its thermal conductivity?

Furthermore, given the fact that the thermal conductivity of slag is strongly influenced by the crystal content of the slag (see Figure 4) and the fact that Campforts *et al.*[10] demonstrated that freeze-linings typically consisted of complex layers of glass and crystals—under initial conditions of formation

(Figure 2)—we pose a further question, to what extent would the *crystal content* of *manganese-bearing* slag influence its thermal conductivity?

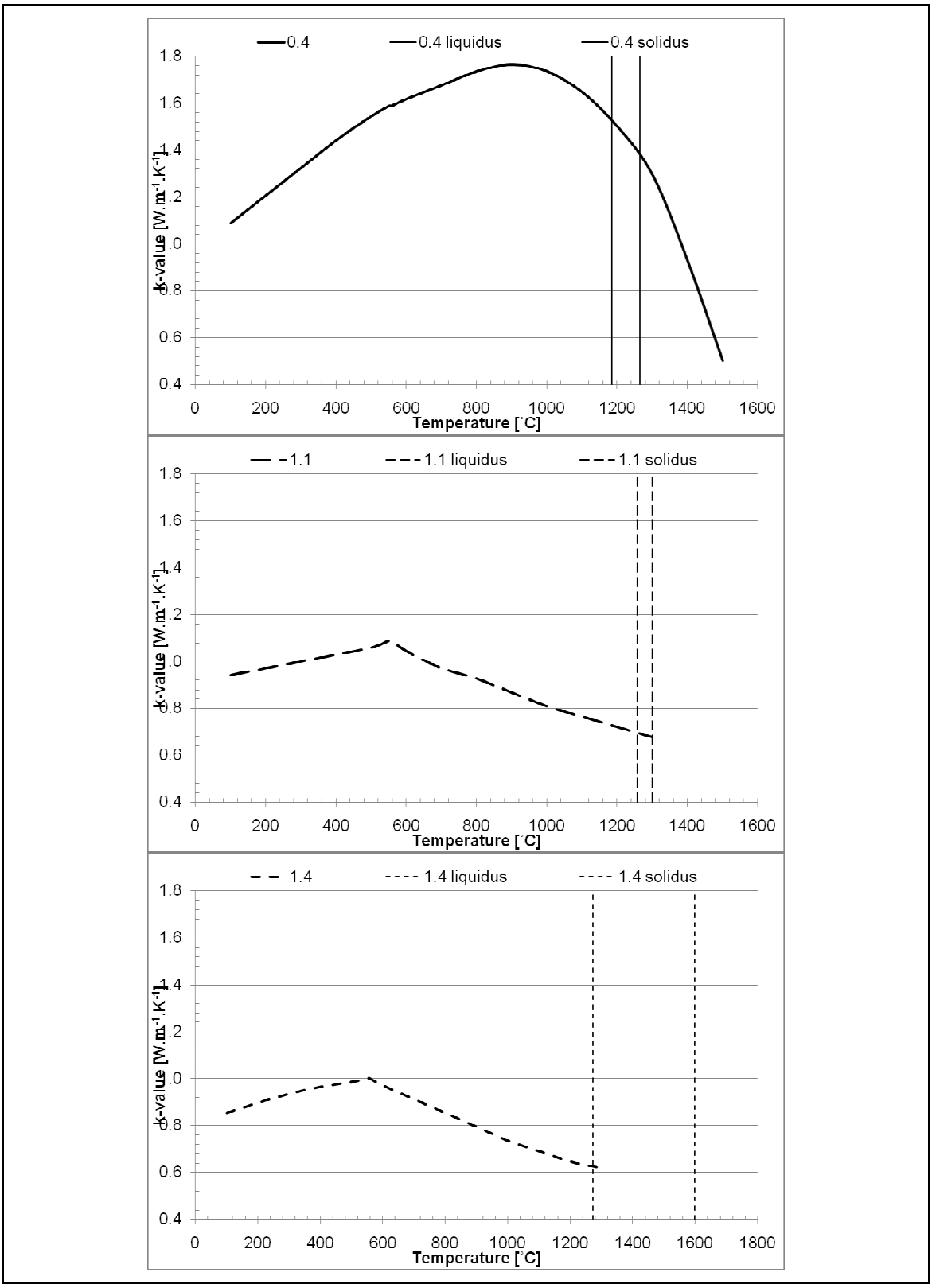

Figure 5: Measured thermal conductivities of the Al_2O_3-CaO-SiO_2 system at a fixed Al_2O_3 content of 15% by mass and various ratios of CaO:SiO_2 (per cent by mass) of 0.4, 1.0 and 1.4 (redrawn from Mills and Susa[9]). Vertical lines indicate the solidus and liquidus of each slag composition as calculated by FACTSage 6.1 with the FACT53 and FToxid databases.

Finally, given the fact that the thermal conductivity of slag is strongly influenced by slag chemistry—as depicted by the dependence on basicity (as in Figure 5)—and the fact that different types of manganese-bearing slags will have different compositions (Table I) where basicity could be expressed according to Equation 1 or Equation 2, we pose the question, to what extent would the *chemistry* of different types of *manganese-bearing* slags influence their thermal conductivity?

In this paper we report and examine the first results of the study.

SAMPLE PREPARATION

Crushed MnO-rich, industrial slag (slag A) was melted in a graphite crucible in air in an ASEA induction furnace. Temperature, related to power input, was monitored with a type-S thermocouple. When the slag temperature remained stable at 1450°C for 5 minutes, the power was switched off.

The melting temperature of 1450°C was selected based on the expected slag composition and calculations in FACTSage (Table I). The liquidus temperature calculation for slag A (1323°C) was based on its actual composition indicated in Table II. The melting temperature therefore exceeded the liquidus temperature of slag A by more than 100°C ensuring that the slag was completely molten upon casting.

The molten slag was cast into a slag pot made of graphite in an attempt at cooling the slag at varying cooling rates. The technique was inspired by a publication by Kotze and Pistorius, where a photograph of an industrial-scale, high-titania slag block exhibited distinctly different cooling rates (Figure 6a).[11] The attempt was successful, as can be seen by the differences in colour of the glassy (bright green) and crystalline (milky light green) sections in the slag block broken in two in Figure 6b.

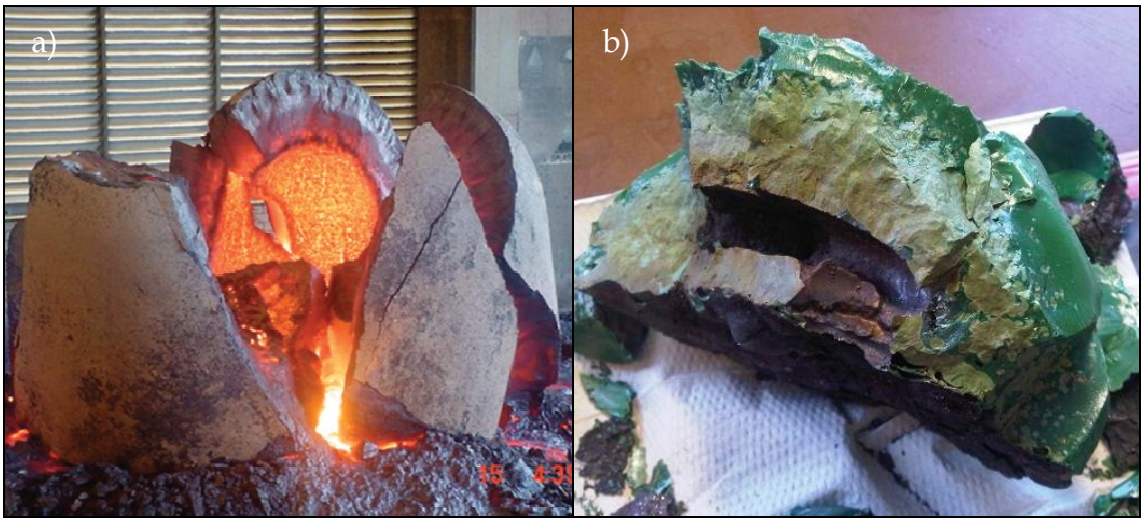

Figure 6: (a) Industrial-scale, high-titania slag block exhibiting distinctly different cooling rates (after Kotze and Pistorius)[11] and(b) slag A after melting and casting, exhibiting distinctly different crystal structures due to different cooling rates similar to the high-titania slag block.

The chemical composition of slag A after melting was determined by X-ray fluorescence (XRF) spectrometry (ARL9400XL) with pressed-powder briquettes. Samples were prepared from both the glassy (dark green slag in Figure 6b) and crystalline sections (light green slag in Figure 6b). A blank, certified material was analysed with the samples. The results were simplified to a five component slag—all other components in the slag being 1% or less—and normalised (see Table II).

Table II: Chemical composition of slag determined by XRF (mass per cent)

		SiO_2	Al_2O_3	MnO	MgO	CaO	B_2	B_5	T_{sol}† (°C)	T_{liq}† (°C)
Slag A, after melting	Average	24	16	36	4	20	0.8	1.5	1106	1323
	Glassy	24	16	36	4	20	0.8	1.5	1106	1323
	Crystalline	25	15	36	4	20	0.8	1.5	994	1302
Slag B		27	13	38	6	16	0.6	1.5	1004	1275

† The solidus (T_{sol}) and liquidus (T_{liq}) temperature of each slag composition, as calculated with FACTSage 6.1 and the FACT53 and FToxid databases.

To obtain an idea of the mineral composition of slag A after melting and casting, samples prepared from both the glassy (dark green slag in Figure 6b) and crystalline sections (light green slag in Figure 6b), were analysed by X-ray diffractometry (XRD).

The crushed and milled samples were analysed in a PANalytical X'Pert Pro powder diffractometer with X'Celerator detector. The divergence and receiving slits, directing Mn-filtered Fe-Kα radiation, were variable. The phases were identified with X'Pert Highscore plus software. Twenty per cent Si was added (as a standard) to determine the amorphous content. The results are reported in Table III.

Table III: Phase composition of slag A and slag B determined by XRD (mass per cent)

Mineral	Stoichiometry	Slag A, glassy	Slag A, crystalline	Slag B
Amorphous	–	83	13	16
Gehlenite	$Ca_2Al(AlSiO_7)$	–	7	–
Olivine (glaucochroite)	$CaMnSiO_4$	–	57	62
Spinel	$(Mn, Mg)Al_2O_4$	–	10	16
Manganosite	(Mn, Mg, Ca)O	17	13	6

To determine the thermal conductivity of slag A, the laser flash analysis technique was used. The technique required two types of sample:

1. For linear expansion measurements ($\Delta L/L$) a rectangular-shaped sample were prepared. The sample had to be 5 mm high, 5 mm wide and 25 mm long.
2. For thermal diffusivity measurements (α) disk-shaped samples were prepared. Samples had to have a diameter of 10 mm and thickness of

2 mm. These samples had to be free of cracks and pores and the smooth surfaces had to be parallel.

To prepare the samples, slag A was cut and core drilled, sliced and polished using standard geological sample-preparation equipment. The idea was to prepare samples that consisted only of glassy (dark green slag in Figure 6b) material and samples that consisted only of crystalline (light green slag in Figure 6b) material. Sample preparation posed major challenges as the slag samples tended to disintegrate upon drilling. In the end, three crack-free and pore-free, disk-shaped samples were prepared from slag A. A suitable rectangular-shaped sample could not be prepared from slag A. The disk-shaped samples consisted of glassy and crystalline regions, but in different concentrations. It was impossible to prepare samples that consisted only of glassy material or only of crystalline material. Two samples were selected for laser-flash analysis (see Figure 7).

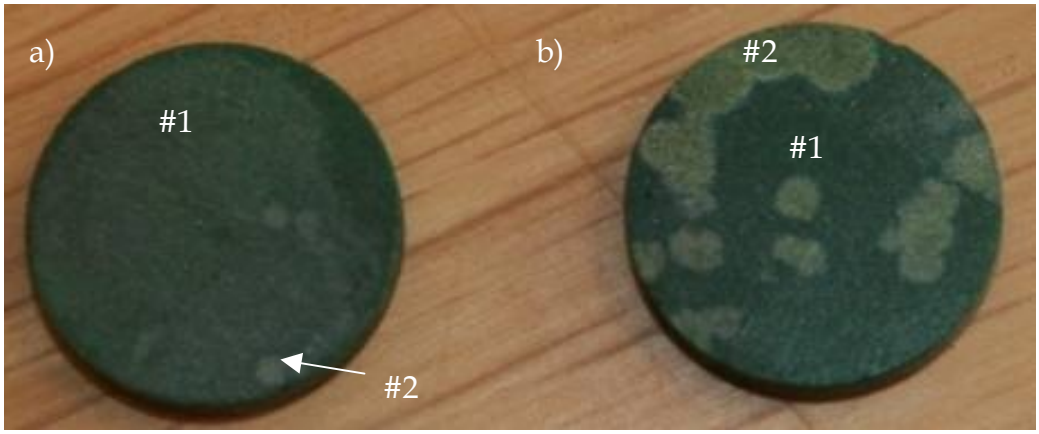

Figure 7: Samples of slag A—10 mm in diameter prior to laser-flash measurements—with #1 the glassy structure and #2 is the crystalline structure.

From the XRD results in Table III, the glassy slag A appeared not to be 100% glassy and the crystalline slag A not to be 100% crystalline. To obtain a better understanding of the mineral composition of the glassy and crystalline sections of the samples prepared for laser-flash analysis, a third disk-shaped sample was mounted and polished. The mounted and polished sample was examined with a Nikon Eclipse E200 petrographic microscope (Figure 8) and a JEOL JSM 6300 scanning electron microscope (SEM) with energy dispersive spectroscopy (EDS).

The micrograph in Figure 8a indicates that the glassy material consisted of large dendritic crystals in an amorphous matrix. SEM-EDS indicated that the dendrites consisted of 95% MnO, 4% MgO and 1% CaO, a composition consistent with manganosite reported for slag A in Table III. The micrograph in Figure 8b indicates that the crystalline material also contained large dendritic crystals, but this time in a crystalline matrix. In this instance, too, SEM-EDS confirmed that the dendrites consisted of 95%MnO, 4%MgO and 1% CaO. At this stage two different phases could be differentiated in the crystalline matrix, but only the bulk analysis could be confirmed by SEM-EDS. No evidence of

amorphous material in the matrix could be found. The amorphous material in the crystalline material reported by XRD (Table III) was most probably present because of an error introduced during sampling.

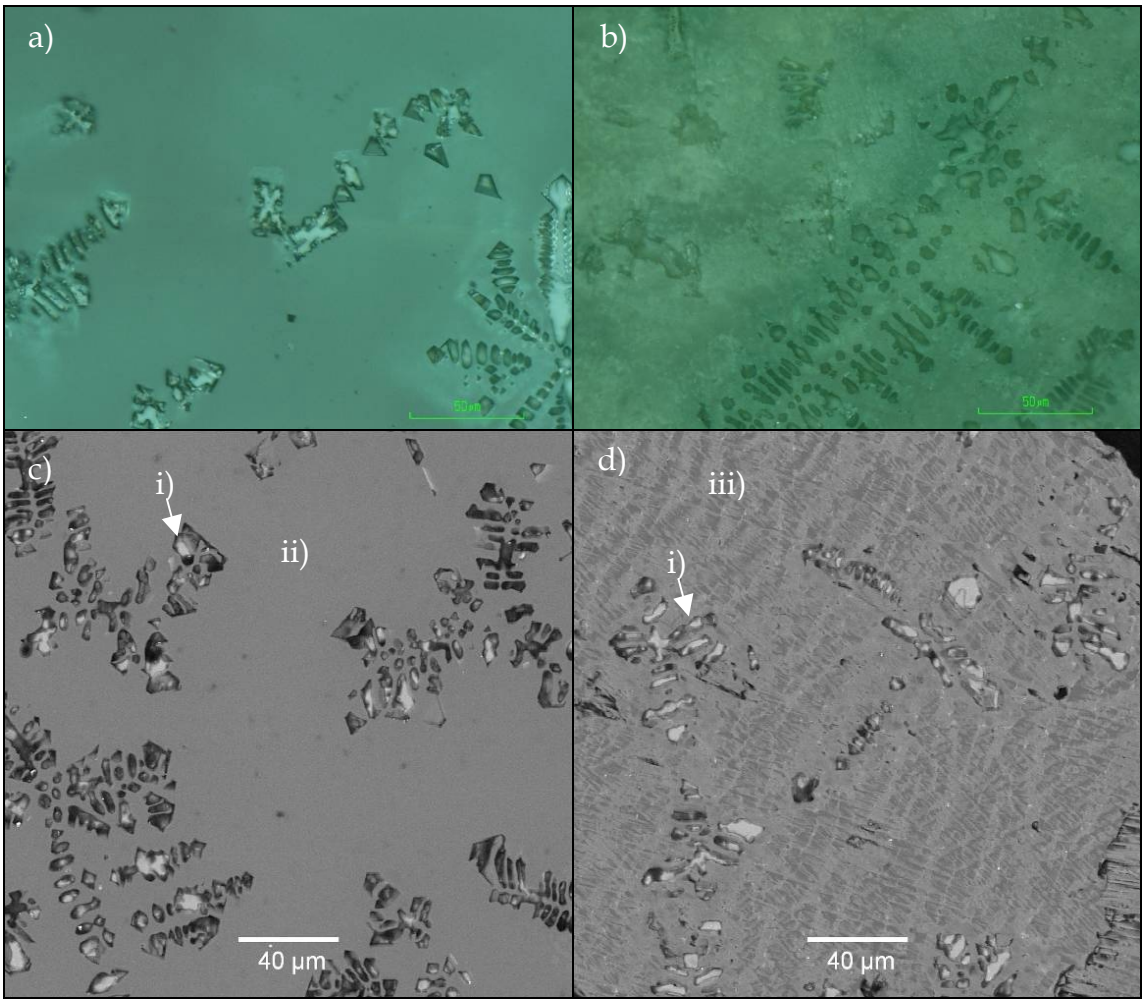

Figure 8: Micrographs taken with a petrographic microscope of (a) the glassy and (b) crystalline structures of slag A and SEM backscattered-electron micrographs of (c) the glassy and (d) crystalline structures. (i) Manganosite, (ii) amorphous matrix, and (iii) crystalline matrix.

To estimate the phase composition of the two samples selected for laser flash analysis, the fraction glassy material and fraction crystalline material in each sample was estimated and correlated with the XRD data. To correlate the results Equation 3 and Equation 4 were used. In both equations, x is the fraction of crystalline material in the sample. Equation 3 and Equation 4 are based on the assumption that the fraction of crystalline material in each sample does not contain any amorphous material.

$$\%glass = 0.83 \times (1 - x) \quad [3]$$

$$\%crystal = 0.17 \times (1 - x) + x \quad [4]$$

To estimate the fraction of crystalline material in each sample (x), photographs of both sides of the samples (see Figure 7) were taken with a CANON EOS30D camera. For each side of a sample the percentage surface area of the crystalline region was measured with ImageJ image analysis software.[12] The average of measurements on each side of the sample was calculated. It was assumed that

this average surface area represented the fraction of crystalline regions of each sample. The sample in Figure 7a contained 4% (slag A#1) crystalline material and the sample in Figure 7b contained 24%. The estimations are summarised in Table IV.

Table IV: Estimated glassy- and crystalline-material content of the two disk-shaped slag A samples

Material	Glassy	Crystalline
Slag A#1	80%	20%
Slag A#2	63%	37%

Although not ideal, a second sample of industrial, MnO-rich slag was introduced into the study, as thermal conductivity measurements of slag A could not be done without a suitable rectangular-shaped sample. Slag B was a slow-cooled, crystalline sample produced during a pilot smelting campaign. From slag B three disk-shaped samples and one rectangular-shaped sample were prepared. Two were selected for laser-flash analysis (slag B#1 and slag B#2) and the third was mounted and polished. The chemical composition and phase composition of slag B were determined in a similar fashion to those of slag A. The compositions are presented in Table II and Table III, respectively.

The two samples selected for laser-flash analysis were not photographed before subjecting them to the analysis, but the third sample, mounted and polished, was photographed (see Figure 9). The sample was examined under a petrographic microscope (see Figure 10) and by SEM with EDS. We see from Figure 10a that slag B consisted of several crystalline phases. Small, bright white spots of a metallic phase were observed as well. These were not detected by XRD (Table III), which has a detection limit of between 1% and 2%.

Figure 9: Sample of slag B, 10 mm in diameter prior to laser-flash measurements. Note the small metallic particles (bright white spots).

From the SEM-EDS analysis the light grey crystals (i) in Figure 10 were identified as manganosite with a composition of 96% MnO, 3% MgO and 1% CaO; the dark grey crystals in Figure 10ii, as spinel with a composition of 58% Al_2O_3, 30% MnO and 12% MgO; and the grey matrix (iii) in Figure 10,

consisting of 26%SiO_2, 49%MnO, 22%CaO and 3%MgO, potentially as a mixture of MnO (manganosite) and $CaMnSiO_4$ (olivine).

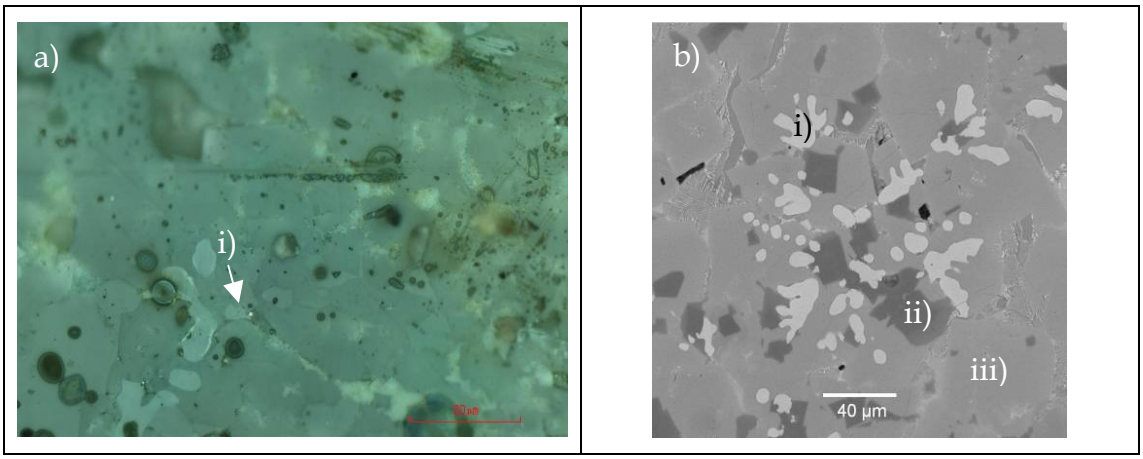

Figure 10: Micrographs taken with a petrographic microscope of (a) slag B. (i) a small, bright white spot, identifies a metallic particle. SEM backscattered-electron image of (b) slag B. (i) identifies manganosite, (ii) spinel and (iii) a matrix analysing 26%SiO_2, 49%MnO, 22%CaO and 3%MgO.

THERMAL CONDUCTIVITY MEASUREMENTS

The laser-flash method was utilised to determine the coefficient of thermal conductivity (k, $W.m^{-1}.K^{-1}$) of the samples as a function of temperature. By this method the coefficient of thermal conductivity is calculated from the density (ρ, $kg.m^{-3}$), specific heat capacity (Cp, $J.kg^{-1}.K^{-1}$), and diffusivity (a, $mm^2.s^{-1}$) of a specific sample according to Equation 5:[13]

$$k(T) = \rho(T).Cp(T).\alpha(T) \quad [5]$$

The density as a function of temperature depended on the reference density (ρ_{ref}, $kg.m^{-3}$) and measured linear expansion ($\Delta L/L$), according to Equation 6:[14]

$$\rho(T) = \frac{\rho_{ref}}{\left(1+\frac{\Delta L}{L}(T)\right)^3} \quad [6]$$

The reference density of each sample is based on room temperature measurements of mass (m, kg), thickness (h, m) and diameter (d, m); it is calculated according to Equation 7:[14]

$$\rho_{ref} = \frac{m}{\pi(\frac{d}{2})^2 h} \quad [7]$$

Densities are reported in Table V. As slag compositions are similar, the significant difference in density of the slag A and slag B samples are attributed to the presence of small metallic particles observed in Figure 10a. Small metallic particles may not have been observed in the slag A samples (Figure 8) because re-melting allowed the dense metal to separate from the slag (Figure 11).

Table V: Density of slag samples at room temperature (ρ_{ref})

Sample	Density [kg.m^{-3}]
Slag A, 4% crystalline matter	3.4
Slag A, 24% crystalline matter	3.4
Slag B #1	3.6
Slag B #2	3.6

Figure 11: Removing HCFeMn metal that collected at the bottom of the graphite slag pot during cooling of Slag A. The metal was entrapped in the as-received industrial slag during tapping and separated from the slag during re-melting because of the difference in density between the metal and the slag.

The linear expansion ($\Delta L/L$) was measured from room temperature to 1000°C in a Netzsch 402E dilatometer at a heating rate of 2°C.min^{-1} in air. As only one rectangular-shaped sample could be prepared and only from slag B, only one set of results were obtained. The results are plot in Figure 12. A linear curve fits the results with an R^2 of 0.999.

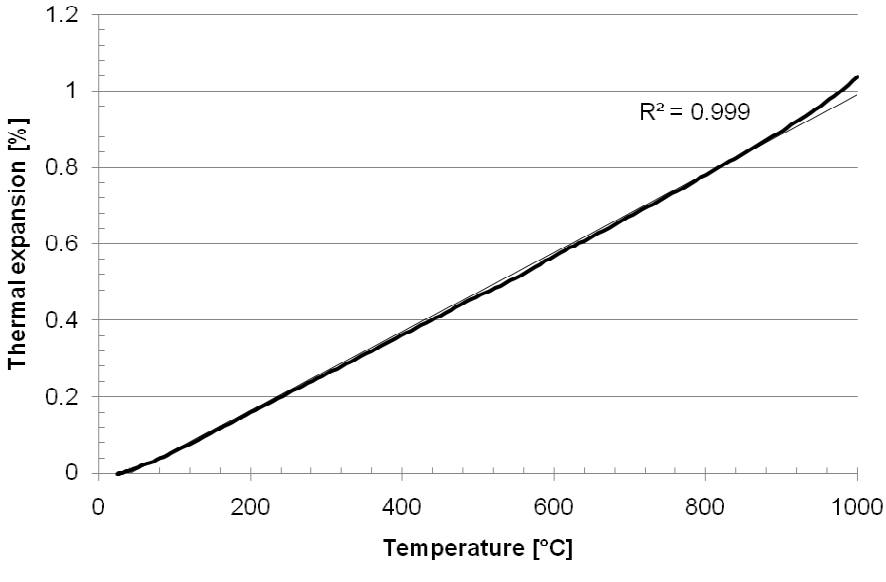

Figure 12: Thermal expansion of slag B

The coefficient of linear expansion (α_L) for slag B, quantified as 10.3 × 10^{-6} °C^{-1}, was calculated from the dataset in Equation 8:[15]

$$\frac{\Delta L}{L} = \alpha_L \Delta T \qquad [8]$$

The linear expansion results for slag B were used in the calculation of the coefficients of thermal conductivity of both the slag A and slag B samples, but as the major phases in the slags are the same (as shown below) the thermal expansion coefficients are expected not to differ significantly.

The specific heat capacity (Cp) and thermal diffusivity (α) as a function of temperature were measured in a Netzsch LFA 457 Microflash. Samples were heated from room temperature to 1000°C in nitrogen; measurements were taken at 100°C intervals. The sample heating rate was 10°C.min^{-1} from room temperature to 100°C and 20°C.min^{-1} from 100°C to 990°C. The heat capacities of the slag samples were measured against the Pyroceram 9606 reference sample (see Figure 13). The α results are presented in Figure 14.

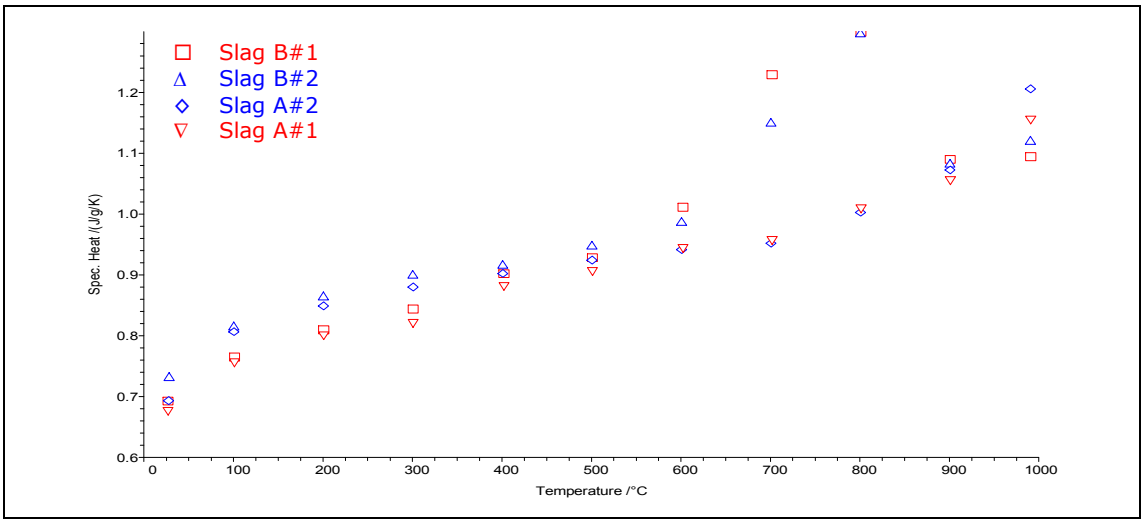

Figure 13: Specific heat capacities of slag A and slag B

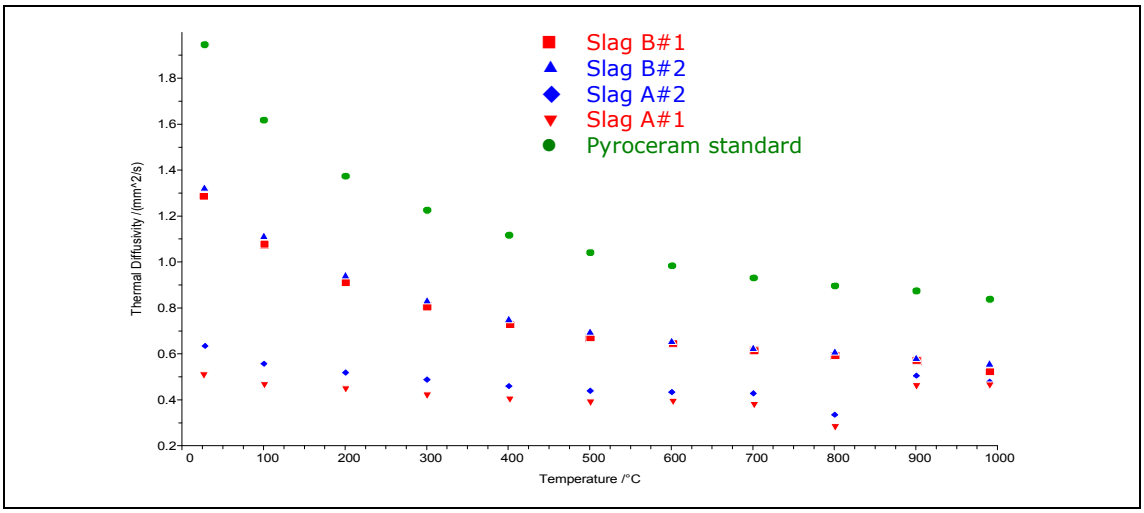

Figure 14: Thermal diffusivities of slag A and slag B

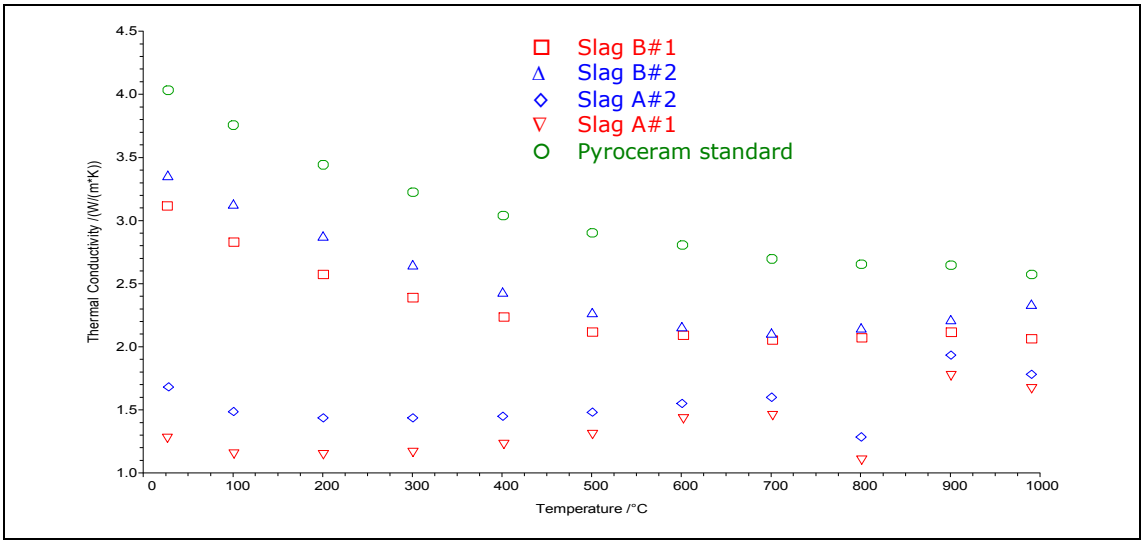

Figure 15: Thermal conductivities of slag A and slag B

Proteus® 4.8.5 software was used to calculate the thermal conductivity (*k*) of the slag samples. The Cowan regression model was applied (see Figure 15).

In the *Cp* results (Figure 13), the *a* results (Figure 14), and the *k* results (Figure 15) something happened at 800°C. Photographs were taken (with a CANON EOS 30D camera and 100 mm Tamron macro lens) of sections through slag A before (Figure 16a) and after (Figure 16b) laser-flash measurement. The glassy material in slag A recrystallized during laser flashing (Figure 16b, point i). The recrystallization probably took place at about 800°C, but follow-up investigations are required.

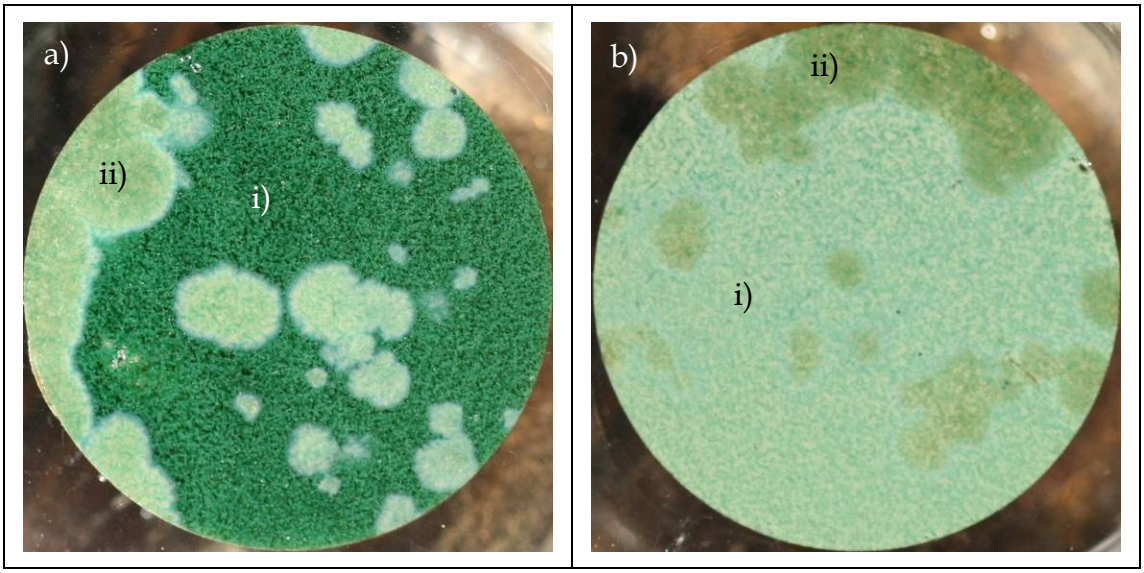

Figure 16: Samples of slag A, 10 mm in diameter, (a) before being laser flashed and (b) after being laser flashed. In (a), point i is a glassy material and point ii the crystalline material. In (b) point i is the glassy structure which recrystallised into a crystalline structure and point ii the original crystalline structure.

LIMITATIONS OF THE DATASET

1. Having only one set of linear expansion results introduces two uncertainties in the measurements:
   i. The first uncertainty is the reproducibility of the results. To what extent will linear expansion data of a second or third sample of slag B, match the data in Figure 12?
   ii. The second uncertainty is the difference in crystal content between the slag A and slag B samples. To what extent will linear expansion data of slag A, match the linear expansion data of slag B?
2. The small, metallic particles present in slag B will most probably increase the thermal diffusivity and therefore thermal conductivity of the slag.
3. Thermal conductivity measurements were limited to 1000°C, a limitation posed by the equipment available. From the results of the simplified calculation in Figure 3 the temperature range across a freeze lining will range from ~200°C at the cold face to the melting temperature of the slag at its hot face. The effect of temperature on the thermal conductivity of the freeze lining in the temperature range 1000°C to melting temperature remains unknown.

CONCLUSIONS

A method was developed to quantify the effect of crystal content on the thermal conductivity of rich HCFeMn slag. Bearing in mind the limitations of the dataset described above, we make some preliminary observations:

1. The thermal diffusivity, and therefore thermal conductivity, of industrial, rich HCFeMn slag is dependent on temperature at temperatures ranging from room temperature to 990°C
2. The crystal content of industrial, rich HCFeMn slag has a significant influence on the thermal diffusivity, and therefore thermal conductivity, at temperatures ranging from room temperature to 990°C

The dependency of thermal conductivity on temperature and crystal content will have a significant influence on the thickness—and potentially stability—of the freeze-lining in submerged-arc furnaces.

To produce definitive measurements of the thermal conductivity of rich HCFeMn slag, the quality of the data should be improved by taking the following steps:

1. Ideally, a sample should consist either of glassy or of crystalline material
2. For each type of material—glassy or crystalline—the linear expansion of at least two but ideally three samples should be measured. The calculated average should be used in thermal conductivity calculations.
3. Linear expansion results for the crystalline material should not be used in thermal conductivity calculations of glassy material, and vice versa
4. To ensure that small, metallic particles do not interfere with thermal diffusivity measurements and thermal conductivity results, samples should be prepared from synthetic-slag mixtures

5. One of the reviewers recommended that microporosity measurements be included in the characterisation of the slag

To improve the predictive quality of calculations when designing furnace containment systems, the thermal conductivity of rich HCFeMn slag should be measured from ~200°C at the cold face to ~1447°C, the melting temperature of the slag at the hot face.

ACKNOWLEDGMENTS

The contributions of our colleagues are gratefully acknowledged, specifically those of Jeanette Dykstra, Michal Ksiazek, Wiebke Grote, Johan de Villiers, and Jacques Muller, as well as the contributions of the peer reviewers of the paper.

REFERENCES

1. F. Habashi (ed.), *Handbook of extractive metallurgy*, 1997, vol. 1, Wiley-VCH, pp. 420–434.
2. S.E. Olsen, M. Tangstad and T Lindstad, *Production of manganese ferroalloys*, 2007, Tapir Academic Press, pp. 49–53.
3. P.L. Duncanson and J.D. Toth, The truths and myths of freeze lining technology for submerged arc furnaces, *INFACON X: Transformation through Technology*, 1–4 February 2004, pp. 488–499.
4. A.M. Hearn, A.S.J. van Rensburg and J.R. Henning, "Freeze" lining on M12 furnace: motivation, installation and operation, *INFACON X: Transformation through technology*, 1–4 February 2004, pp. 500–507.
5. A.M. Hearn, A.J. Dzermejko and P.H. Lamont, "Freeze" lining concepts for improving submerged arc furnace lining life and performance, *8th International Ferroalloys Congress*, Beijing, China, 7–10 June 1998, pp. 401–426.
6. K. Verscheure et al, Furnace cooling technology in pyrometallurgical processes, *Sohn International Symposium: Advanced processing of metals and materials*, volume 4 New, improved and existing technologies: Non-ferrous materials extraction and processing, 2006, pp. 139–154.
7. A.G. Matyas et al, Application of new technology in the design of high-power electric smelting furnaces, *CIM Bulletin*, vol. 86, 1993, pp. 92–99.
8. J.D. Steenkamp, M. Tangstad and P.C. Pistorius, Importance of thermal conductivity of manganese bearing slags in design of freeze lining systems. Paper to be submitted to the *J. SAIMM*.
9. K.C. Mills and M. Susa, Thermal conductivities of slags. Slag atlas. 2nd edition. Düsseldorf, Verlag Stahleisen, 1995, pp. 591 (figure 15.17) and 600 (figure 15.23).
10. M. Campforts, B. Blanpain and P. Wollants, The importance of slag engineering in freeze lining applications, *Metall. Mater. Trans., B*, vol. 40, no. 5, 2009, pp. 643–655.
11. H. Kotzé and P.C. Pistorius, A heat transfer model for high titania slag blocks, *J. SAIMM*, vol. 110, 2010, pp. 57–66.
12. http://rsbweb.nih.gov/ij/
13. ASTM E1461-01: Standard test method for thermal diffusivity by the flash method.
14. Manual of Netzsch LFA 457 Microflash.
15. ASTM E228-06 Standard Test Method for Linear Thermal Expansion of Solid Materials With a Push-Rod Dilatometer.
16. C.W. Bale, P. Chartrand, S.A. Degterov, G. Eriksson, K. Hack, R. Ben Mahfoud, J. Melançon, A.D. Pelton and S. Petersen, FactSage thermochemical software and databases, *CalPhad*, vol. 26, 2002, pp. 189–228.
17. Y. Lee and D. Deming, Evaluation of thermal conductivity temperature corrections applied in terrestrial heat flow studies, *J. Geophys. Res.*, vol. 103, 1998, pp. 2447–2454.

Joalet Dalene Steenkamp

Senior lecturer, University of Pretoria

Joalet holds three degrees in engineering (B.Eng., B.Eng. (Hons) and M.Eng.) from the University of Pretoria. She is currently enrolled for a PhD in Engineering under the supervision of Professor Pistorius and Professor Tangstad. The work presented here forms part of her PhD study. Joalet joined the University of Pretoria as a member of the academic staff in January 2009. Her prior employment included various technical positions at Exxaro Resources (Kumba / Iscor) and Richard's Bay Minerals.

Joalet registered as professional engineering with ECSA in 2002 and was elected as a member of the SAIMM in 2009.

In her spare time Joalet is an amateur photographer, her husband, son and two dogs being her favourite, and sometimes willing, subject matter.